Table 1. Plasma samples

	n
No malignant tumors	17
<1 year	11
>1 year	6
Neuroblastomas	756
Stage 1,2,4S	372
Stage 3,4	330
Unknown	54
MYCN amplification –	643
MYCN amplification +	97
Unknown	16
High *TrkA* expression	425
Low *TrkA* expression	159
Unknown	172
Mass screening	387
Sporadic	286
Stage 1,2,4S	62
Stage 3,4	209
Unknown	15
MYCN amplification –	207
MYCN amplification +	73
Unknown	6
High *TrkA* expression	109
Low *TrkA* expression	113
Unknown	64
Hyperdiploidy/pentaploidy	96
Diploidy/tetraploidy	136
Unknown	54
<18 months	101
>18 months	183
Unknown	2
Unknown	83
Hyperdiploidy/pentaploidy	379
Diploidy/tetraploidy	263
Unknown	114
<18 months	506
>18 months	242
Unknown	8

blocked with 300 μL of 0.1% casein, 0.01% Microcide I (aMReSCO) in PBS for 20 h at 37 C. Plasma samples (10 μL each) were mixed with 100 μL of 50 mM Tris HCL (pH 8.4), 0.5 M KCl, 0.1% casein, 0.5% bovine serum albumin (BSA), 0.01% Microcide I and 0.1 μg/mL peroxidase-labeled chicken antihuman MK antibody. Aliquots of 50 μL of this mixture were added to wells prepared as described above, and further subjected to chromogenic detection at optical density at 450 nm (OD_{450}) using tetramethylbenzidine as the substrate. This assay system shows linearity from 0 to 5 ng/mL of MK, and there is no cross-reaction with pleiotrophin, a close homolog of MK.[5]

Statistical analysis. The Kruskal–Wallis test was used to evaluate the statistical differences between stages. The Mann–Whitney *U*-test was used to further evaluate the difference between the two groups. The Mann–Whitney *U*-test was used for analysis of the other prognostic factors. Survival time was measured from the date of initial diagnosis to the date of death or last contact. The Kaplan–Meier method was used to compare survival between the groups defined by plasma MK levels, and survival differences were analyzed using the log-rank test. All analyses were carried out using StatView for Windows (ver. 5.0; SAS Institute, Cary, NC, USA). $P < 0.05$ was considered statistically significant.

Results

Plasma MK levels of NBL patients and the relationship of plasma MK to established prognostic factors for NBL. The entire set of 756 NBL cases consisted of 387 cases found through mass screening, 286 sporadic NBL cases and 83 unknown cases (Table 1). Plasma MK level of the NBL cases was 23–1 062 520 pg/mL, whereas that of non-tumor controls was 146–517 pg/mL (Fig. 1a). The values of NBL cases were significantly higher than those of controls ($P < 0.0001$). We set the cut-off value average ± 4SD of non-tumor controls at 900 pg/mL (Fig. 1a). The group of cases with levels higher than 900 pg/mL was designated high MK, whereas cases with lower than 900 pg/mL were grouped into low MK.

MYCN amplification, *TRKA* expression level, ploidy, stage and age are well-known prognostic factors for NBL.[1] The values of each factor were determined for all 756 NBL cases. As shown in Figure 1(b–f), MK levels were significantly correlated with all the prognostic factors. Thus, MK levels were significantly higher in *MYCN*-amplified cases ($P < 0.0001$, *versus MYCN*-nonamplified), in cases with low *TRKA* expression ($P < 0.0001$, *versus* high *TRKA* expression), in diploidy cases ($P = 0.004$), in cases at stage 3 and 4 ($P < 0.0001$, *versus* stage 1, 2, and 4S) and in cases older than 18 months ($P < 0.0001$, *versus* younger than 18 months). These groups in which MK levels were high, i.e. *MYCN*-amplified, low *TRKA* expression, diploidy, stage 3 and 4 and older than 18 months, are known to have a poor prognosis. The data indicate close correlations between MK levels and known prognosis factors and are consistent with our previous report.[15]

Figure 2(a) shows Kaplan–Meier survival curves based on plasma MK levels for all NBL cases. A high MK level was closely associated with poor prognosis of NBL patients ($P < 0.0001$), indicating that the MK level alone can be a prognostic factor for NBL patients. It was interesting that a high MK level was associated with poor prognosis within the unfavorable NBL group based on ploidy, i.e. diploidy ($P = 0.02$) (Fig. 2b). This was also the case within favorable NBL groups, that is, groups with *MYCN* non-amplification, age <18 months or high *TRKA* expression ($P = 0.02$, 0.001 or 0.02, respectively), although the survival differences between high MK and low MK were very small (data not shown).

Analysis for sporadic NBL cases. We examined 286 sporadic NBL cases, among which prognostic information was available for only 175. Plasma MK level was significantly higher in sporadic NBL cases than in non-tumor controls ($P < 0.0001$) (Fig. 3a). It was closely related to the values of two prognostic factors, i.e. *MYCN* amplification and stage ($P = 0.0005$ and 0.003, respectively) (Fig. 3b,c), but not to those of age, *TRKA* expression level and ploidy (data not shown).

Kaplan–Meier analysis revealed that a high MK level was correlated with poor prognosis in the sporadic NBL patients ($P = 0.04$) (Fig. 4a). The Kaplan–Meier data on MK was further compared with those on known prognostic factors. Survival based on ploidy exhibited a significant difference ($P = 0.025$) (Fig. 4b). *MYCN* amplification, *TRKA* expression level and stage also showed significant differences ($P = 0.003$, 0.01 and 0.008, respectively), whereas age could not be a prognostic factor for the sporadic NBL cases examined (data not shown). The Cox hazard ratio was 1.71 for MK level, 2.27 for ploidy, 2.70 for *MYCN* amplification, 2.38 for *TRKA* expression and 1.84 for stage.

Discussion

In the present study, we first evaluated the plasma MK level using the entire set of NBL cases including both the mass screening and sporadic cases. As predicted from our previous data,[15] we found that MK level is correlated with established prognostic factors (*MYCN*, *TRKA*, ploidy, stage and age). Since

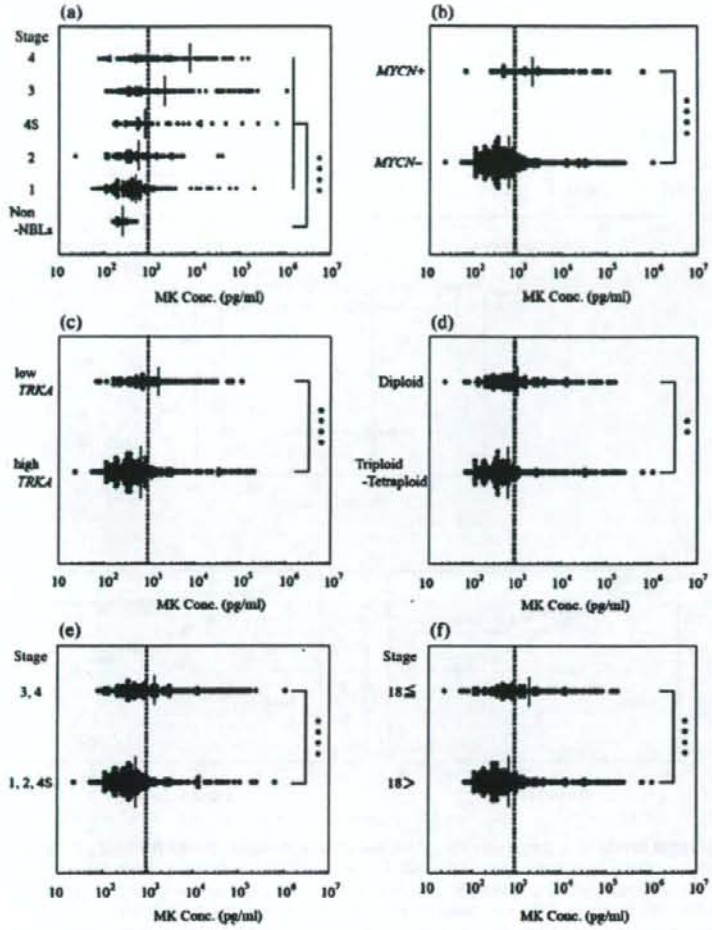

Fig. 1. Plasma midkine (MK) levels of the entire set of neuroblastoma (NBL) cases and the relationship of MK level to established prognostic factors for NBL. Blood MK levels are presented with dots. Each dot represents a NBL patient or a non-NBL control as indicated. (a) MK level distribution of the NBL patients through stages. Non-NBL, non-NBL controls. $^{****}P < 0.0001$. (b) NBL cases divided into *MYCN* amplification (MYCN+) and nonamplification (MYCN–). $^{****}P < 0.0001$. (c) NBL cases divided into low *TRKA* expression (low *TRKA*) and high *TRKA* expression (high *TRKA*). $^{****}P < 0.0001$. (d) NBL cases divided into diploid and triploid/pentaploid. $^{**}P = 0.004$. (e) NBL cases divided into stage 3 or 4 (Stage 3, 4) and stage 1, 2 or 4S (Stage 1, 2, 4S). $^{****}P < 0.0001$. (f) NBL cases divided into age >18 months and <18 months. $^{****}P < 0.0001$.

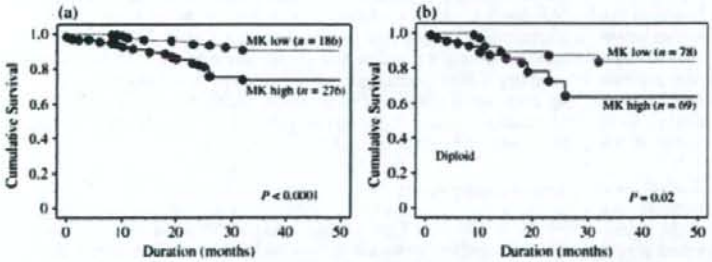

Fig. 2. Kaplan–Meier curves for neuroblastoma (NBL) cases. 'MK low' was defined as a blood midkine (MK) level less than 900 pg/mL, whereas 'MK high' was more than 900 pg/mL. Cumulative survival rates of MK low and high groups were estimated for the entire set of NBL cases (a) and cases with diploidy (b).

mass screening has been discontinued, sporadic NBL are the major subject of therapy. We therefore further evaluated the MK level of only the sporadic cases. Our study revealed that, within sporadic cases, blood MK level alone could be a predictor of prognosis. MK level was also significantly correlated with *MYCN* amplification and stages.

However, blood MK level could not predict prognosis of patients in the intermediate risk group (*MYCN* non-amplification and stage 3 or 4) (data not shown). It could not predict the prognosis of patients within the high-risk group or low-risk group either (data not shown). This indicates that a single molecule may not be satisfactory for predicting the prognosis or judging the precise status of NBL for the decision of therapy, since, like other carcinomas, a complex of molecules is thought to contribute to carcinogenesis and development of NBL.[17,18] There are several blood markers predicting clinical outcome of neuroblastoma patients; i.e. serum lactate dehydrogenase, ferritin, neuron-specific enolase, disialoganglioside GD2 and NM23H1.[19–23] Therefore,

doi: 10.1111/j.1349-7006.2008.00957.x

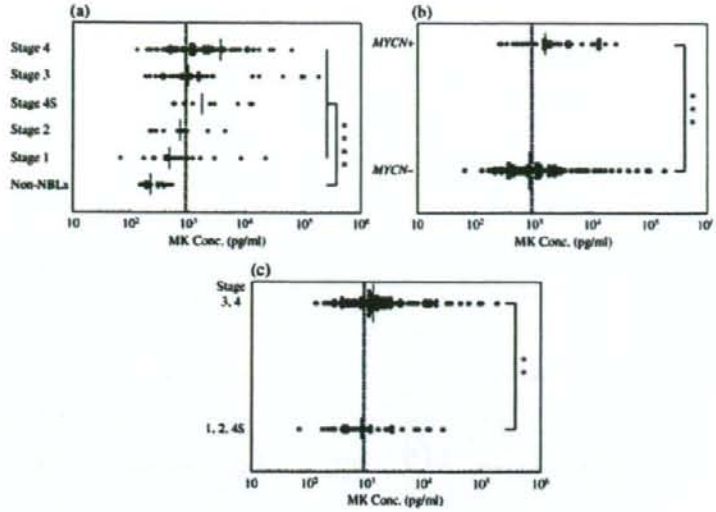

Fig. 3. Analysis for sporadic neuroblastoma (NBL) cases. Blood midkine (MK) levels of sporadic NBL cases are shown. (a) MK level distribution of the sporadic NBL patients through stages. Non-NBLs, non-NBL controls. $^{****}P < 0.0001$. (b) Sporadic NBL cases divided into *MYCN* amplification (MYCN+) and non-amplification (MYCN–). $^{***}P = 0.0005$. (c) Sporadic NBL cases divided into stage 3 or 4 (Stage 3, 4) and stage 1, 2 or 4S (Stage 1, 2, 4S). $^{**}P = 0.003$.

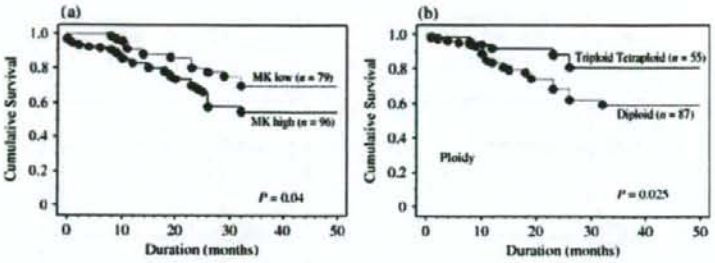

Fig. 4. Kaplan–Meier curves for sporadic neuroblastoma (NBL) cases. Cumulative survival rates of sporadic NBL cases were compared based on the following criteria. (a) Midkine (MK) low or high. (b) Diploid or triploid/pentaploid.

it is reasonable to expect that a combination of the plasma levels of MK and other blood biomarkers will facilitate accurate prognosis and accurate evaluation of tumor status. In addition, many efforts are being made to identify molecular changes associated with NBL with unfavorable prognosis.[17,18] Such studies will provide other biomarkers for NBL.

It is interesting that MK levels of stage 4s were lower in the present study than those in the previous study. Twelve cases were only available for stage 4s in the previous study. In the present study, 39 cases of stage 4s were available for the analysis of the entire set of NBL (Fig. 1a) and 15 cases for the sporadic NBL (Fig. 3a). Therefore, it is conceivable that midkine level deduced in the present study is more reliable because of the increased number of cases analyzed.

This is the first report indicating the plasma MK level as a prognosis factor for a human carcinoma. MK is frequently and highly expressed in malignant tumors regardless of the tissue type,[5] similar to mutations in the p53 gene. An elevated serum MK level is also detected in more than 80% of human adult carcinomas.[16] Although the MK level has not been evaluated as a prognosis factor for human carcinomas except for NBL, further assessment of the MK level will be useful in potentially establishing it as a new biomarker for other carcinomas.

Tumor growth is suppressed by the knockdown of MK expression.[13,14] MK is barely detectable in normal adult tissues. Furthermore, the present study has established that high blood MK level is closely related to poor prognosis, at least in NBL. Therefore, our data also support the idea that MK is a candidate molecular target for cancer therapy. Indeed, MK-deficient mice carrying a *MYCN* transgene show delayed development of NBL as compared with wild-type mice (Kishida and Kadomatsu, unpublished data). A therapy targeting MK for NBL is currently being studied in our laboratory.

Acknowledgments

We thank Tohru Doi for a critical reading of this manuscript. This work was supported by Grants-in-Aid from the Ministry of Education, Science, Sports, Culture (15COEF01-09, 18790218) and a Grant-in-Aid from the Ministry of Health (CAN16K16).

References

1 Brodeur GM. Neuroblastoma: biological insights into a clinical enigma. *Nat Rev Cancer* 2003; 3: 203–16.
2 Henry MC, Tashjian DB, Breuer CK. Neuroblastoma update. *Curr Opin Oncol* 2005; 17: 19–23.
3 Kadomatsu K, Tomomura M, Muramatsu T. cDNA cloning and sequencing of a new gene intensely expressed in early differentiation stages of embryonal carcinoma cells and in mid-gestation period of mouse embryogenesis. *Biochem Biophys Res Commun* 1988; 151: 1312–18.
4 Tomomura M, Kadomatsu K, Nakamoto M *et al.* A retinoic acid responsive gene, MK, produces a secreted protein with heparin binding activity. *Biochem Biophys Res Commun* 1990; 171: 603–9.
5 Kadomatsu K, Muramatsu T. Midkine and pleiotrophin in neural development and cancer. *Cancer Lett* 2004; 204: 127–43.
6 Tsutsui J, Kadomatsu K, Matsubara S *et al.* A new family of heparin-binding

growth/differentiation factors: increased midkine expression in Wilms' tumor and other human carcinomas. *Cancer Res* 1993; **53**: 1281–5.
7 Aridome K, Tsutsui J, Takao S *et al.* Increased midkine gene expression in human gastrointestinal cancers. *Jpn J Cancer Res* 1995; **86**: 655–61.
8 Mishima K, Asai A, Kadomatsu K *et al.* Increased expression of midkine during the progression of human astrocytomas. *Neurosci Lett* 1997; **233**: 29–32.
9 O'Brien T, Cranston D, Fuggle S *et al.* The angiogenic factor midkine is expressed in bladder cancer, and overexpression correlates with a poor outcome in patients with invasive cancers. *Cancer Res* 1996; **56**: 2515–18.
10 Garver RI Jr, Radford DM, Donis-Keller H *et al.* Midkine and pleiotrophin expression in normal and malignant breast tissue. *Cancer* 1994; **74**: 1584–90.
11 Ye C, Qi M, Fan QW *et al.* Expression of midkine in the early stage of carcinogenesis in human colorectal cancer. *Br J Cancer* 1999; **79**: 179–84.
12 Konishi N, Nakamura M, Nakaoka S *et al.* Immunohistochemical analysis of midkine expression in human prostate carcinoma. *Oncology* 1999; **57**: 253–7.
13 Takei Y, Kadomatsu K, Matsuo S *et al.* Antisense oligodeoxynucleotide targeted to Midkine, a heparin-binding growth factor, suppresses tumorigenicity of mouse rectal carcinoma cells. *Cancer Res* 2001; **61**: 8486–91.
14 Takei Y, Kadomatsu K, Itoh H *et al.* 5′-,3′-inverted thymidine-modified antisense oligodeoxynucleotide targeting midkine. Its design and application for cancer therapy. *J Biol Chem* 2002; **277**: 23 800–6.
15 Ikematsu S, Nakagawara A, Nakamura Y *et al.* Correlation of elevated level of blood midkine with poor prognostic factors of human neuroblastomas. *Br J Cancer* 2003; **88**: 1522–6.
16 Ikematsu S, Yano A, Aridome K *et al.* Serum midkine levels are increased in patients with various types of carcinomas. *Br J Cancer* 2000; **83**: 701–6.
17 Ohira M, Oba S, Nakamura Y *et al.* Expression profiling using a tumor-specific cDNA microarray predicts the prognosis of intermediate risk neuroblastomas. *Cancer Cell* 2005; **7**: 337–50.
18 Wamat P, Oberthuer A, Fischer M *et al.* Cross-study analysis of gene expression data for intermediate neuroblastoma identifies two biological subtypes. *BMC Cancer* 2007; **7**: 89–99.
19 Joshi VV, Cantor AB, Brodeur GM *et al.* Correlation between morphologic and other prognostic markers of neuroblastoma. A study of histologic grade, DNA index, N-myc gene copy number, and lactic dehydrogenase in patients in the Pediatric Oncology Group. *Cancer* 1993; **71**: 3173–81.
20 Hann HW, Levy HM, Evans AE. Serum ferritin as a guide to therapy in neuroblastoma. *Cancer Res* 1980; **40**: 1411–3.
21 Zeltzer PM, Marangos PJ, Parma AM *et al.* Raised neuron-specific enolase in serum of children with metastatic neuroblastoma. A report from the Children's Cancer Study Group. *Lancet* 1983; **2**: 361–3.
22 Valentino L, Moss T, Olson E *et al.* Shed tumor gangliosides and progression of human neuroblastoma. *Blood* 1990; **75**: 1564–7.
23 Okabe-Kado J, Kasukabe T, Honma Y *et al.* Clinical significance of serum NM23-H1 protein in neuroblastoma. *Cancer Sci* 2005; **96**: 653–60.

doi: 10.1111/j.1349-7006.2008.00957.x

Vascular endothelial growth factor expression is closely related to irinotecan-mediated inhibition of tumor growth and angiogenesis in neuroblastoma xenografts

Setsuko Kaneko, Makiko Ishibashi and Michio Kaneko[1]

Department of Pediatric Surgery, Graduate School of Comprehensive Human Sciences, University of Tsukuba, Tsukuba, Ibaraki 305-8575, Japan

(Received September 18, 2007/Revised January 25, 2008/Accepted January 31, 2008/Online publication March 31, 2008)

In the present study, irinotecan (CPT-11) was highly effective not only against the chemosensitive neuroblastoma (NB) xenografts SK-N-AS*nu* and TNB9, but also against the multidrug-resistant NB xenograft TS-N-2*nu*. SK-N-AS*nu* and TNB9 were significantly more responsive to low-dose daily CPT-11 treatment than to intermittent administration of one-third of the median lethal dose. For TS-N-2*nu*, there was no significant difference in tumor growth inhibition between the two treatment schedules. Treatment with CPT-11 alone could not completely abolish tumor growth in mice. For TNB9, tumor regrowth seemed to result from an inability to regress host vessels in the stroma during treatment and an inability to suppress host-derived vascular endothelial growth factor (VEGF) expression throughout therapy. In the multidrug-resistant TS-N-2*nu*, VEGF was not suppressed by low-dose therapy with CPT-11, and neurofilament-positive tumor cells escaped from apoptosis and were growth arrested at G_0/G_1 phase. These findings suggest a mechanism for the incomplete responsiveness of TS-N-2*nu* to CPT-11. Our data demonstrate that diminished VEGF gene and protein expression is closely correlated with tumor growth inhibition and inhibition of angiogenesis by CPT-11 in NB xenografts. Our results further suggest that a persistent blocker of stroma-derived VEGF will need to be combined with CPT-11 to completely inhibit the growth of chemosensitive NB, and that administration of CPT-11 at higher doses will be required to inhibit the growth of multidrug-resistant NB. (*Cancer Sci* 2008; 99: 1209–1217)

Neuroblastoma is one of the most common malignant solid tumors in childhood. There have been significant advances in the treatment of NB. However, the treatment results for patients older than 1 year of age with disseminated disease and those with *MYCN*-amplified NB are still unsatisfactory. Among the newly developed antitumor drugs with therapeutic activity, CPT-11 is promising for NB treatment.[1–4] CPT-11 is a semisynthetic derivative of camptothecin,[5] and exerts antitumor activity by inhibiting DNA topoisomerase I.[6] Topotecan, a camptothecin analog, has been shown to inhibit transcriptional activity and protein accumulation of HIF-1α in human glioma cells by a DNA damage-independent mechanism, and to cause significant tumor growth inhibition in glioblastoma xenografts.[7,8] HIF-1 is a transcription factor that plays a major role in cellular adaptive responses to hypoxia. It is a heterodimer composed of the HIF-1α and HIF-1β subunits.[9] HIF-1β is expressed constitutively in excess, whereas HIF-1α protein expression is regulated tightly by tissue oxygen concentration. Under normoxia, HIF-1α is degraded rapidly via the ubiquitin–proteasome pathway through prolyl hydroxylation and binding of the von Hippel-Lindau protein. This process is suppressed under hypoxia, allowing increased stability of the HIF-1α protein and transcriptional activation with HIF-1β.[10,11] It has recently been made clear that under hypoxia, HIF-1α accumulates, establishes a feedback loop, and is kept under control by transcription-dependent degradation.[12] Under normoxia, HIF-1α is expressed at low levels. Inhibitors of transcription do not activate the feedback loop. However, under hypoxia, HIF-1α transcriptionally activates its own degradation independent of the prolyl hydroxylase and von Hippel-Lindau pathway. Inhibitors of transcription dramatically superinduce HIF-1α.

More than 60 genes involved in angiogenesis, glycolysis, erythropoiesis, cell survival, and metastasis are activated by HIF-1.[13] The growth and metastasis of solid tumors depends largely on angiogenesis. One of the most important key molecules in the regulation of neoangiogenesis is VEGF.[14] HIF-1α mediates angiogenesis by induction of VEGF.[15–17]

In NB, high *VEGF* gene expression correlates with stage IV of the disease.[18] High tumor vascularity is associated with disseminated disease, *MYCN* amplification, unfavorable histology, and poor outcome.[19,20] Therefore, inhibiting VEGF expression and interfering with angiogenesis may be a useful treatment target for aggressive NB. To date, there have been no reports investigating the relationship between tumor growth inhibition, inhibition of HIF-1α and VEGF gene and protein expression, and inhibition of histopathological angiogenesis in NB. Using three human NB xenografts, we evaluated the antitumor activity of CPT-11 administered intermittently at one-third of the LD_{50} and continually at low doses. We further investigated the relationship between the inhibition of tumor growth, inhibition of HIF-1α and VEGF gene and protein expression, and inhibition of histological angiogenesis by CPT-11 in chemosensitive and multidrug-resistant NB xenografts.

Materials and Methods

Animals and human NB xenografts. Human NB xenografts designated TNB9 and TS-N-2*nu* were derived from stage IV NB with 80 and 13 copies of *MYCN* amplification in the adrenal gland of a 15-month-old boy and the adrenal of a 4-year-old girl, respectively. Our preparatory studies confirmed that the original biological characteristics of TNB9 and TS-N-2*nu*, particularly *MYCN* amplification status and chromosome findings, were retained after serial transplantations. The SK-N-AS NB cell line, generously donated by Dr Tohru Sugimoto (Kyoto Prefectural University of Medicine), was maintained in RPMI-1640 medium supplemented

[1]To whom correspondence should be addressed.
E-mail: mkaneko@md.tsukuba.ac.jp

Abbreviations: CPT-11, irinotecan; HIF, hypoxia-inducible factor; LD_{50}, the median lethal dose; MIR, maximal growth inhibition rate; NB, neuroblastoma; NF, neurofilament protein; NSE, neuron-specific enolase; RTW, relative tumor weight; SMA, smooth muscle actin; TUNEL, terminal deoxynucleotidyl transferase-mediated dUTP-biotin nick-end labeling; VEGF, vascular endothelial growth factor.

doi: 10.1111/j.1349-7006.2008.00790.x

with 10% fetal bovine serum (BioWest, Nuaille, France). SK-N-AS cells have no *MYCN* amplification. The NB xenograft designated SK-N-AS*nu* was generated by injecting $\sim 1 \times 10^6$ cultured SK-N-AS cells subcutaneously into the flank of Balb/cAJcl-nu mouse (CLEA Japan, Tokyo, Japan), and the tumor generated was passaged several times before treatment.

Some small pieces of minced tumor were implanted subcutaneously with trochars into the unilateral or bilateral flanks of 5–6-week-old male nude mice. Treatment began in randomized groups of three to six mice when tumors reached approximately 150 mg. Tumor size and mouse bodyweight were measured every 4 days. The tumor weight was calculated according to the formula:

$$\text{tumor weight (mg)} = a \times b^2 \times 1/2,$$

where a is the length of the tumor and b is the width. The mean RTW was calculated using the equation:

$$\text{RTW} = Wx/W0,$$

where Wx and $W0$ are the mean tumor weight on days x and 0 (the initiation of treatment), respectively.

Drug sensitivity of three NB xenografts. Drug sensitivity of SK-N-AS*nu*, TNB9, and TS-N-2*nu* was investigated for eight antitumor drugs: cyclophosphamide, ifosfamide, cisplatin, mitomycin C, vincristine, etoposide, pirarubicin, and CPT-11. Experiments were carried out according to the protocol of Battelle Columbus laboratories.[21,22] Each drug was suspended according to the provider's instructions, and administered intraperitoneally except for pirarubicin, which was administered intravenously. Drugs were administered to six nude mice per group at the total LD_{50} in three injections at 4-day intervals (q4d × 3). Control mice were administered an equivalent volume of vehicle (0.1 mL/10 g bodyweight) intraperitoneally. The MIR was obtained by calculating the minimal ratio of RTW in treated mice (*RTWt*) to that in control mice (*RTWc*) on the same day:

$$\text{MIR} = (1\text{-}RTWt/RTWc) \times 100(\%).$$

Tumor response was evaluated as highly effective (++), effective (+), or ineffective (–) when tumor regression (RTW < 1.0) was seen after treatment, when MIR was equal to or greater than 58%, and when MIR was less than 58%, respectively.

Low-dose prolonged administration of CPT-11. Besides the q4d × 3 schedule of $LD_{50} \times 1/3$ per dose (conventional dose) for the drug-sensitivity experiment, three treatment schedules at a low dose ($LD_{50} \times 1/30$, 5.9 mg/kg per dose) were evaluated: (1) intraperitoneal administration daily for 14 consecutive days (qd × 14); (2) intraperitoneal administration daily for 20 consecutive days (qd × 20); and (3) intraperitoneal administration daily 5 days per week for 2 consecutive weeks followed by a 7-day resting period, with one repetition ([(qd × 5)2]2).

Real-time quantitative reverse transcription–polymerase chain reaction. Total RNA was prepared from frozen tumor tissue according to the acid guanidinium–phenol–chloroform method.[23] One microgram of each RNA sample was incubated with oligo $d(T)_{16}$ and MuLV reverse transcriptase (Applied Biosystems, Foster City, CA, USA) to yield cDNA. The expression levels of the human *HIF-1α* and *VEGF* genes as well as murine *HIF-1α* and *VEGF* genes were measured at the cDNA level by the ABI Prism 7700 Sequence Detection System (Applied Biosystems). Human *β-ACTN* or murine *β-ACTN* was used as an internal control gene. The specific primers used were *hHIF-1α*-f 5′-CCAGTTACGTTCCTTCGATCAGT-3′ and *hHIF-1α*-r 5′-TTTGAGGACTTGCGCTTTCA-3′, *hVEGF*-f 5′-TACCTCCACCATGCCAAGTG-3′ and *hVEGF*-r 5′-ATGATTCTGCCCTCCTCCTTC-3′, *hβ-ACTN*-f 5′-CAACCGCGAGAAGATGACC-3′ and *hβ-ACTN*-r 5′-CACAGCCTGGATAGCAACGTAC-3′, *mHIF-1α*-f 5′-CCAGTTACGTTCCTTTGATCAGT-3′ and *mHIF-1α*-r 5′-GTAACTGTGCTCATACTTGGA-3′, *mVEGF*-f 5′-AACGATGAAGCCCTGGAGT-3′ and *mVEGF*-r 5′-CCGCATGATCTGCATGGT-3′, *mβ-ACTN*-f 5′-AGACTTCGAGCAGGAGATGG-3′ and *mβ-ACTN*-r 5′-TCAGGCAGCTCATAGCTCTTC-3′. The sequences of the TaqMan probes were *hHIF-1α* 5′-FAM-CACCATTAGAAAGCAGTTCCGCAAGCC-TAMRA-3′, *hVEGF* 5′-FAM-TCCCAGGCTGCACCCATGGC-TAMRA-3′, *hβ-ACTN* 5′-FAM-TTTGAGACCTTCAACACCCCAGCCA-TAMRA-3′, *mHIF-1α* 5′-FAM-CACCATTAGAGAGCAATTCTCCAAGCC-TAMRA-3′, *mVEGF* 5′-FAM-TGCCCACGTCAGAGAGCAACAT-TAMRA-3′, and *mβ-ACTN* 5′-FAM-CACTGCCGCATCCTCT-TCCTCCCT-TAMRA-3′. Twenty microliters of the polymerase chain reaction mixture used for quantification contained template cDNA, 1× qPCR Mastermix (Eurogentec, San Diego, CA, USA), 300 nM of each primer, and 200 nM of TaqMan probe. Each experiment was carried out in triplicate and repeated twice. The thermal cycling conditions were: 50°C for 2 min, 95°C for 10 min, 45 cycles at 95°C for 15 s, and 60°C for 1 min.

Immunoblotting. Frozen tumor samples were crushed in liquid nitrogen and homogenized in a sample buffer consisting of 125 mM Tris-HCl (pH 6.8), 20 mM dithiothreitol, 4% sodium dodecylsulfate, 10% glycerol, and 0.5% protease inhibitor cocktail (Complete Mini; Roche Applied Science, Mannheim, Germany). The extracts were sonicated for 10 s and centrifuged at 17 000*g* for 10 min at 4°C to remove debris. The protein concentrations were determined using the Bio-Rad DC protein assay (Bio-Rad Laboratories, Hercules, CA, USA). Samples containing the same amounts of protein (10–70 μg) were separated on 12.5% sodium dodecylsulfate–polyacrylamide gels, electroblotted on polyvinylidene fluoride membranes (Immobilon-P; Millipore, Bedford, MA, USA), and probed with antibodies. The primary antibodies used were anti-HIF-1α clone H1α67 (Novus Biologicals, Littleton, CO, USA) at a dilution of 1:1000, anti-VEGF clone A-20 (Santa Cruz Biotechnology, Santa Cruz, CA, USA) at a dilution of 1:900, and anti-actin clone 20–33 (Sigma, St Louis, MO, USA) at a dilution of 1:500. Bound antibodies were detected with horseradish peroxidase-conjugated secondary antimouse (Amersham Biosciences, Buckinghamshire, UK) or antirabbit (Stressgen, Victoria, BC, Canada) antibodies, followed by an enhanced chemiluminescence system (PerkinElmer Life Sciences, Boston, MA, USA).

Immunohistochemistry and detection of apoptotic cells. Tumors were fixed in 10% neutral buffered formalin for 24 h prior to paraffin embedding. After deparaffinization, tissue sections were heated at 121°C for 7–30 min either in 50 mM citrate buffer (pH 6.0) for NSE and NF, or in 10 mM Tris buffer with 1 mM ethylenediaminetetraacetic acid (pH 9.0) for αSMA and Ki-67 antigen. Endogenous peroxidase was blocked with 3% hydrogen peroxide in methanol for 3 min at room temperature. Anti-NSE (Sigma) and monoclonal anti-Ki-67 antigen clone MIB-1 (DakoCytomation, Carpinteria, CA, USA) were in their ready-to-use forms. A monoclonal anti-NF clone 2F11 (Dako, Glostrup, Denmark) and a monoclonal anti-αSMA clone 1A4 (Dako) were used at dilutions of 1:100 and 1:50, respectively. The bound antibodies were amplified using peroxidase-labeled polymer-conjugated antirabbit or antimouse antibody (EnVision+ System; DakoCytomation). For the coloring reaction, 3,3′-diaminobenzidine (Sigma) was used as the chromogen and nuclear counterstaining was carried out with hematoxylin.

Apoptotic cells in tumor tissues were detected using the TUNEL assay. After deparaffinization and rehydration, tissue sections were covered with 20 μg proteinase K (Wako Pure Chemical Industries, Osaka, Japan) per mL phosphate-buffered saline for 15 min at room temperature. After blocking of endogenous peroxidase, slides were washed in 20 μg proteinase K per mL (PBS) and immersed in TdT buffer (Takara Bio, Shiga, Japan). The samples were then incubated with TdT enzyme (Takara) and biotin-16-dUTP (Roche Applied Science) in the TdT buffer containing 0.01% bovine serum albumin at 37°C for 1.5 h in

doi: 10.1111/j.1349-7006.2008.00790.x

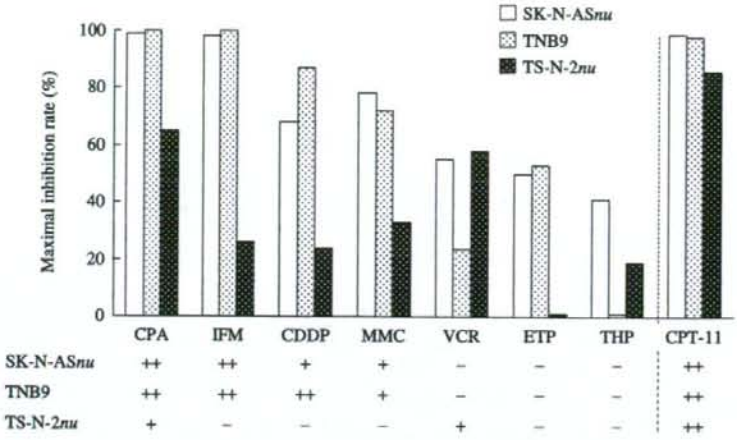

Fig. 1. Maximal growth inhibition rates (MIR) and antitumor effects of eight drugs against three neuroblastoma xenografts. The MIR (%) was obtained by calculating the minimal ratio of mean relative tumor weight (RTW) in treated mice (*RTWt*) over that in control mice (*RTWc*) on the same day. MIR = $(1 - RTWt/RTWc) \times 100$. The antitumor effect was evaluated as highly effective (++) when tumor regression was seen after treatment, effective (+) when the MIR was equal to or greater than 58%, or ineffective (–) and when the MIR was less than 58%. CDDP, cisplatin; CPA, cyclophosphamide; CPT-11; irinotecan; ETP, etoposide; IFM, ifosfamide; MMC, mitomycin C; THP, pirarubicin; VCR, vincristine.

Table 1. Responses of three neuroblastoma xenografts to different irinotecan (CPT-11) treatment schedules

Neuroblastoma xenograft	CPT-11		TD_2 (days)	Maximum decrease in bodyweight (%)
	Dose, schedule	Total dose		
SK-N-AS*nu*	0	0	9.5 ± 2.3	
	59 mg/kg, q4d ×3	LD_{50}	35.5 ± 2.6 **	9
	5.9 mg/kg, qd ×14	$<LD_{50} \times 1/2$	>52.0 **	3
TNB9	0	0	8.9 ± 1.9	
	59 mg/kg, q4d ×3	LD_{50}	25.3 ± 3.8	6
	5.9 mg/kg, ([qd ×5]2)2	$LD_{50} \times 2/3$	22.4 ± 7.6 **	6
	5.9 mg/kg, qd ×20	$LD_{50} \times 2/3$	31.6 ± 2.7 **	2
	5.9 mg/kg, qd ×14	$<LD_{50} \times 1/2$	25.0 ± 2.1	4
TS-N-2*nu*	0	0	10.2 ± 2.6	
	59 mg/kg, q4d ×3	LD_{50}	23.0 ± 2.4 *	4
	5.9 mg/kg, [(qd ×5)2]2	$LD_{50} \times 2/3$	16.6 ± 2.7 *	5
	5.9 mg/kg, qd ×20	$LD_{50} \times 2/3$	21.2 ± 4.3	8

Each treatment schedule of CPT-11 demonstrated significant tumor growth inhibition against three neuroblastoma xenografts ($P < 0.01$, Student's *t*-test). q4d ×3, administration three times at 4-day intervals; ([qd ×5]2)2, administration daily 5 days a week for 2 consecutive weeks, repeated; qd ×20, administered daily for 20 consecutive days; qd ×14, administered daily for 14 consecutive days. LD_{50}, the median lethal dose; TD_2, mean number of days required to reach two times the original tumor weight.
*$P < 0.01$, **$P < 0.001$ by Student's *t*-test. n.s., not significant.

a humidity chamber. Biotin-16-dUTP nucleotides incorporated onto the free 3′ OH ends of DNA fragments were detected using the standard streptavidin–biotin complex immunoperoxidase technique (Elite ABC reagent; Vector Laboratories, Burlingame, CA, USA) with 3,3′-diaminobenzidine as the chromogen.

Statistical analysis. The responses of NB xenografts to CPT-11 were evaluated with respect to tumor growth delay by measuring the mean number of days required to reach two times the original tumor weight for individual tumors. Relative mRNA expression levels for HIF-1α and VEGF were expressed as the mean ± SD. Student's *t*-test or Welch's *t*-test was used to assess the significance of differences between the treatment groups.

Results

Antitumor effects of eight drugs on three NB xenografts. Among the eight antitumor drugs examined, CPT-11 was the most effective when administered at a conventional dose ($LD_{50} \times 1/3$ per dose) at 4-day intervals (Fig. 1). However, CPT-11 has not yet been approved as a therapeutic drug against any pediatric tumors. cyclophosphamide, ifosfamide, cisplatin, and etoposide are standard drugs for NB treatment. SK-N-AS*nu* and TNB9 were sensitive or highly sensitive to all of those drugs except etoposide. TS-N-2*nu* was sensitive to cyclophosphamide, but resistant to the other three drugs. CPT-11 alone was highly effective against TS-N-2*nu*, a multidrug-resistant xenograft. No mice died during that experiment.

Responses of three NB xenografts to intermittent conventional-dose and prolonged low-dose administration of CPT-11. Each treatment schedule for CPT-11 demonstrated significant tumor growth inhibition against the three NB xenografts ($P < 0.01$, Student's *t*-test) without resulting in substantial weight loss in nude mice (Table 1).

Initially, the responses to CPT-11 for a conventional-dose intermittent schedule (q4d × 3) and a low-dose prolonged schedule (qd × 14) were compared in SK-N-AS*nu*. The results are presented in Figure 2a and Table 1. The low-dose qd × 14 schedule was excellent for growth inhibition. Two out of the six tumors treated with low-dose CPT-11 showed complete regression at the end of therapy on day 52. Although the individual total dose for CPT-11 was less than half of LD_{50}, the low-dose qd × 14 schedule was much more efficacious than the conventional-dose

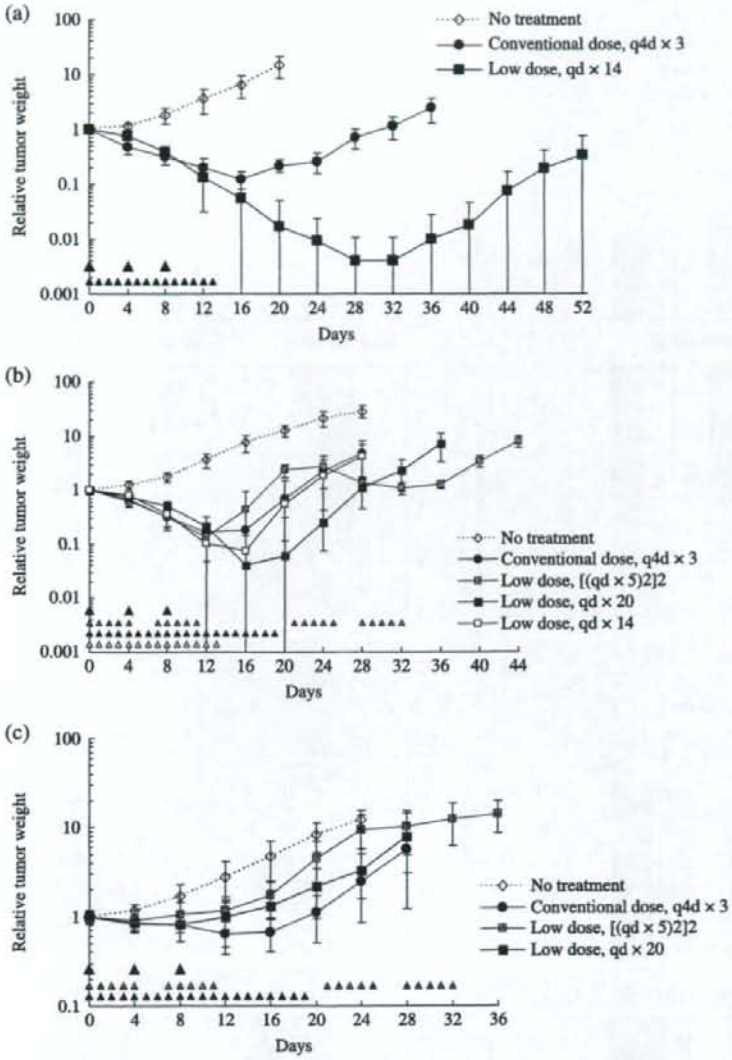

Fig. 2. Responses of (a) SK-N-AS*nu*, (b) TNB9, and (c) TS-N-2*nu* xenografts to irinotecan (CPT-11). Mice were administered CPT-11 intraperitoneally for a conventional-dose (59 mg/kg per dose) intermittent schedule, and for a low-dose (5.9 mg/kg per dose) prolonged schedule. The arrowhead indicates the day CPT-11 was administered. Tumor weight was calculated according to the formula: tumor weight (mg) = $a \times b^2 \times 1/2$, where a is the length of the tumor and b is the width. Tumors were measured every 4 days. The results are presented as mean relative tumor weight ± SD to that on day 0 when treatment was started.

q4d × 3 in which the LD_{50} for CPT-11 was administered ($P < 0.001$, Student's t-test).

The relationship between administration schedules and tumor responses to CPT-11 was further examined using chemosensitive TNB9 and multidrug-resistant TS-N-2*nu* xenografts. TNB9 responded well to all four administration schedules for CPT-11 in the first 2 weeks of treatment (Fig. 2b). Low-dose daily CPT-11 administration without a resting period resulted in a duration-dependent suppression of tumor growth. The low-dose qd × 20 schedule was not only more effective than low-dose qd × 14 ($P < 0.001$, Student's t-test), but also the most effective of all four schedules. It showed significant tumor growth inhibition when compared to conventional-dose q4d × 3 ($P = 0.0077$, Student's t-test), which was as effective as low-dose qd × 14 ($P = 0.890$, Student's t-test). Low-dose ([qd × 5]2)2, in spite of having the longest treatment period at 5 weeks, resulted in rapid tumor regrowth during a 7-day resting period and showed no significant growth delay when compared to conventional-dose q4d × 3 ($P = 0.431$, Student's t-test) or to low-dose qd × 14 ($P = 0.448$, Welch's t-test) (Table 1). These results suggest that CPT-11 administration on a low-dose prolonged schedule without long resting periods is more effective against chemosensitive NB compared with conventional-dose intermittent administration.

In the multidrug-resistant TS-N-2*nu*, no low-dose prolonged schedule showed greater tumor growth inhibition than the conventional q4d × 3 schedule (Table 1; Fig. 2c). There was no significant difference in growth delay between the conventional q4d × 3 and low-dose qd × 20 schedules ($P = 0.412$, Student's t-test). Most tumors did not show increased response to low-dose daily CPT-11 administration throughout treatment. The conventional q4d × 3 schedule was significantly more effective than the low-dose ([qd × 5]2)2, which hardly achieved tumor regression after a 7-day resting period ($P = 0.0029$, Student's t-test) (Table 1). These findings suggest that CPT-11 administered at a higher dose without a long resting period has successful antitumor activity against multidrug-resistant NB.

doi: 10.1111/j.1349-7006.2008.00790.x

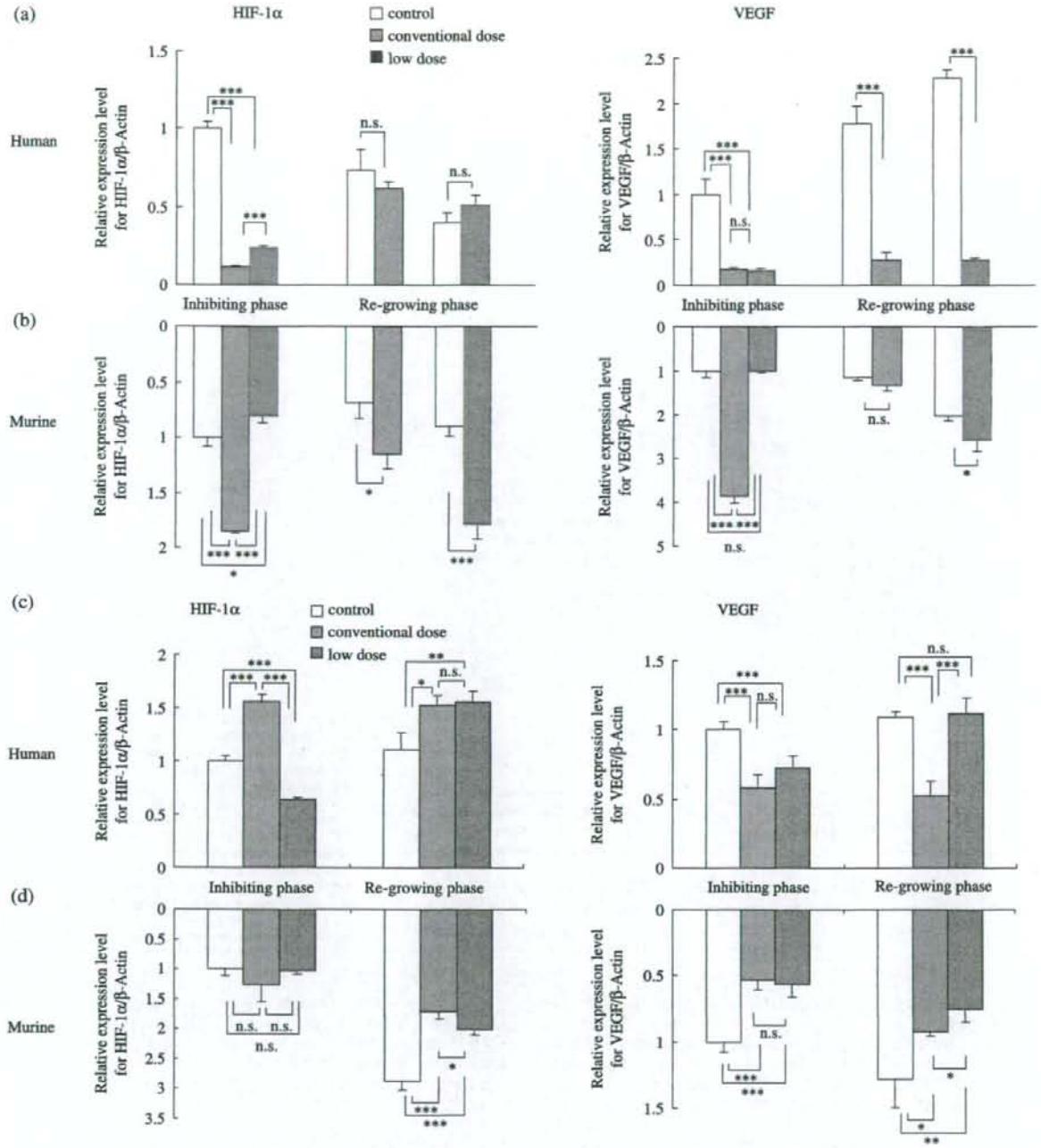

Fig. 3. Quantitative reverse transcription–polymerase chain reaction gene expression analysis of (a,b) TN89 and (c,d) TS-N-2*nu* xenografts. Relative mRNA expression levels for (a,c) human (tumor-derived) and (b,d) murine (host-derived) hypoxia-inducible factor (HIF)-1α and vascular endothelial growth factor (VEGF) in total RNA. Inhibiting phase, tumors on day 10 in TN89, and on day 7 in TS-N-2*nu*. Regrowing phase, tumors on day 14 with conventional-dose treatment and on day 19 with low-dose treatment in TN89, and on day 15 in TS-N-2*nu*. Results are presented as mean relative expression level ± SD to that in untreated tumors in inhibiting phase. $^*P < 0.05$, $^{**}P < 0.01$, $^{***}P < 0.001$; by Student's *t*-test. n.s., not significant.

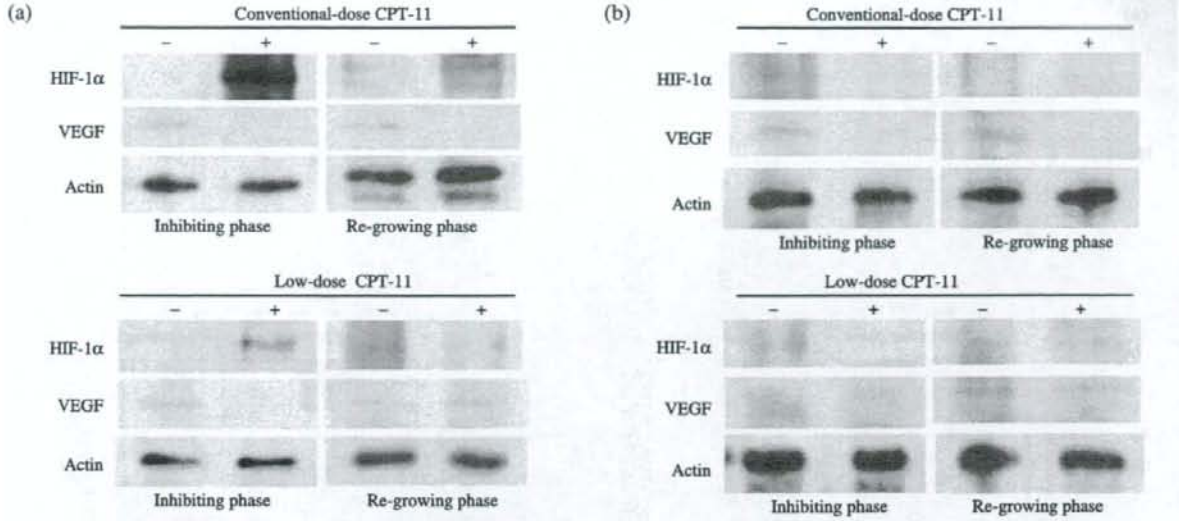

Fig. 4. Immunoblot analysis of hypoxia-inducible factor (HIF)-1α and vascular endothelial growth factor (VEGF) proteins in (a) TNB9 and (b) TS-N-2*nu* xenografts. Inhibiting phase, tumors on day 10 in TNB9, and on day 7 in TS-N-2*nu*. Regrowing phase, tumors on day 14 with conventional-dose treatment and on day 19 with low-dose treatment in TNB9, and on day 15 in TS-N-2*nu*. For protein loading controls, actin levels were checked.

Human and murine *HIF-1α* and *VEGF* gene expression. We quantified human (tumor-derived) and murine (host-derived) *HIF-1α* and *VEGF* gene expression levels in TNB9 and TS-N-2*nu* xenografts (Fig. 3a–d). In the untreated TNB9, the tumor-derived human *HIF-1α* gene expression level was decreased significantly according to the degree of tumor growth (day 10 vs day 14, $P = 0.0331$, Student's *t*-test; day 14 vs day 19, $P = 0.0182$, Student's *t*-test), whereas tumor-derived human *VEGF* gene expression was increased significantly (day 10 vs day 14, $P = 0.0061$, Student's *t*-test; day 14 vs day 19, $P = 0.0020$, Student's *t*-test) (Fig. 3a). Both tumor-derived *HIF-1α* and *VEGF* genes in TNB9 treated with CPT-11 were significantly downregulated regardless of the administration schedule of CPT-11. Gene expression of tumor-derived *HIF-1α* in tumors treated with conventional-dose CPT-11 was reduced significantly compared to tumors treated with low-dose CPT-11 ($P < 0.001$, Student's *t*-test). Suppression of tumor-derived *VEGF* expression was maintained even after the discontinuation of CPT-11 (Fig. 3a). Interestingly, host-derived murine *HIF-1α* and *VEGF* genes in TNB9 treated with conventional doses of CPT-11 were upregulated in a compensatory manner. Host-derived *VEGF* gene expression was not suppressed throughout the course of treatment (Fig. 3b).

In the untreated TS-N-2*nu*, the gene expression levels of tumor-derived human *HIF-1α* as well as *VEGF* remained nearly unchanged regardless of the degree of tumor growth (Fig. 3c). Gene expression of tumor-derived *HIF-1α* in TS-N-2*nu* treated with conventional doses of CPT-11 was upregulated to compensate for inhibition of *VEGF* expression. *VEGF* gene expression was not inhibited by the low-dose daily treatment with CPT-11. Treatment with CPT-11 did not induce host-derived murine *HIF-1α* or *VEGF* gene expression in TS-N-2*nu* (Fig. 3d).

These results demonstrate that in NB xenografts treated with CPT-11, there is a close relationship between the gene expression levels of tumor-derived *VEGF* and the degree of tumor growth inhibition, regardless of the administration schedule. In TNB9, host-derived HIF-1α and VEGF produced by the host stroma throughout the course of CPT-11 therapy appear to be responsible for rapid tumor regrowth. In contrast, in TS-N-2*nu*, host-derived *HIF-1α* and *VEGF* gene expression seem to contribute less to tumor regrowth.

Hypoxia-inducible factor-1α and VEGF protein expression in NB xenografts. In TNB9, HIF-1α protein was induced dramatically during conventional-dose treatment with CPT-11, whereas VEGF protein expression was inhibited (Fig. 4a). HIF-1α protein expression was reduced to a level almost as low as that observed in untreated tumors after 1 week of conventional-dose therapy. At that time, VEGF protein expression was still inhibited. Low-dose daily CPT-11 treatment did not cause strong induction of HIF-1α protein, although expression was not inhibited (Fig. 4a). VEGF protein in tumor treated with daily low doses of CPT-11 was induced soon after the discontinuation of CPT-11.

In TS-N-2*nu*, HIF-1α protein expression was not induced strongly throughout CPT-11 treatment. Intermittent conventional, but not low-dose daily, treatment with CPT-11 strongly inhibited VEGF protein expression (Fig. 4b).

These findings demonstrate that strong induction of HIF-1α protein with inhibition of VEGF protein expression in TNB9 is caused by conventional-dose CPT-11 treatment, and that HIF-1α protein expression is not always inhibited by low-dose daily CPT-11 treatment. These results suggest that VEGF but not HIF-1α protein expression is related to inhibition of tumor growth.

Histology and immunohistochemistry. The anti-αSMA antibody reacts with the smooth muscle of blood vessels. Tumor endothelial microvessels are completely covered by a layer of αSMA-positive pericytes.[24] Therefore, we identified tumor vessels in NB xenografts via αSMA immunostaining.

Untreated TNB9 contained poorly differentiated, NSE-positive tumor cells with fibrovascular stroma (Fig. 5a, left panels). The density of the vessels increased according to the degree of tumor growth (data not shown). TNB9 treated daily with low doses of CPT-11 showed obvious necrosis, calcification, and fibrosis. Nests of NSE-positive tumor cells were scattered among the peripheral fibrous capsules (Fig. 5a, middle panels). Immunostaining for αSMA showed high vascularity in the stromal areas. Soon after low-dose CPT-11 therapy, nests of viable tumor cells were

doi: 10.1111/j.1349-7006.2008.00790.x

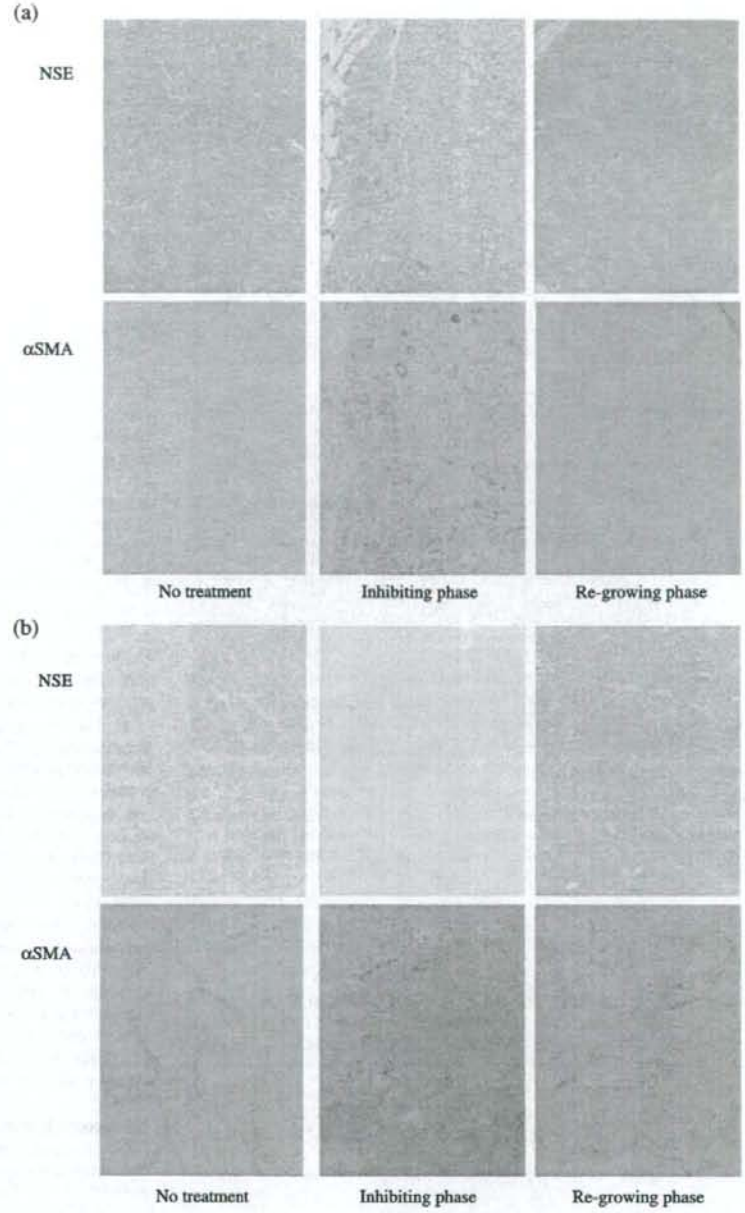

Fig. 5. Immunohistochemistry of (a) TNB9 and (b) TS-N-2*nμ* xenografts during CPT-11 treatment. Tumor sections from mice without CPT-11 treatment, in inhibiting phase, and in regrowing phase were stained using the immunoperoxidase technique for neuron-specific enolase (NSE) and α-smooth muscle actin (SMA). (Original magnification, ×60.) (a) Untreated TNB9 contained poorly differentiated NSE-positive tumor cells with fibrovascular stroma (left panels). In inhibiting phase, nests of NSE-positive tumor cells were scattered among the peripheral fibrous capsules. High vascularity was observed in the stromal areas (middle panels). In regrowing phase, nests of viable tumor cells were dominant with sparse necrotic areas, and tumor vascularity was reduced (right panels). (b) Untreated TS-N-2*nu* contained uniform NSE-positive tumor cell masses intermingled with microvessels that had developed in the fibroconnective stroma (left panels). In tumors in inhibiting phase, the number of NSE-positive cells was markedly diminished, and a small number of large vessels was scattered in the stromal area (middle panels). Tumors in regrowing phase showed limited areas of necrosis, calcification, and connective tissue stroma. Large vessels were seen in the stroma (right panels).

dominant with sparse necrotic areas, and tumor vascularity was reduced (Fig. 5a, right panels).

Untreated TS-N-2*nu* contained uniform NSE-positive tumor cell masses intermingled with microvessels that had developed in the fibroconnective stroma (Fig. 5b, left panels). TUNEL-positive apoptotic cells were seen sparsely in the tumor (data not shown). In TS-N-2*nu* treated with conventional doses of CPT-11, wide areas of necrosis, calcification, and stromal ingrowth were observed. The number of NSE-positive cells was diminished markedly, and a small number of large vessels was scattered in the stromal area (Fig. 5b, middle panels). TS-N-2*nu* treated daily with low doses of CPT-11 showed limited areas of necrosis, calcification, and connective tissue stroma. Large vessels were seen in the stroma (Fig. 5b, right panels). TS-N-2*nu* treated daily with low doses of CPT-11 strongly expressed NF and contained a large number of apoptotic cells. Immunohistochemical findings for NF, TUNEL, and Ki-67 antigens in mirror sections of TS-N-2*nu* treated daily with low doses of CPT-11 revealed that NF-positive cells had escaped from apoptosis (Fig. 6a,b). Furthermore, nearly all NF-positive cells were negative for Ki-67 (Fig. 6c,d), which indicated that they were arrested at the G_0/G_1 phase.[25]

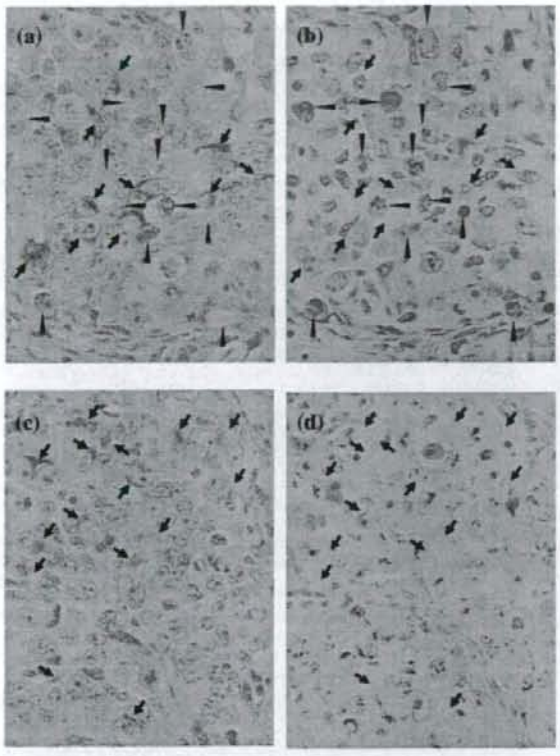

Fig. 6. Immunohistochemistry for (a,c) neurofilament protein (NF), (b) terminal deoxynucleotidyl transferase-mediated dUTP-biotin nick-end labeling and (d) Ki-67 antigen in mirror sections of TS-N-2*nu* treated with low-dose qd×15. (Original magnification, ×300.) (a,b) NF-positive cells (arrows) escaped from apoptosis (arrowheads). (c,d) Nearly all NF-positive cells (arrows) were negative for Ki-67 and arrested at G_0/G_1 phase.

Discussion

Most anticancer drugs cause DNA damage and inhibit tumor cell proliferation. They are usually administered at high doses to kill as many tumor cells as possible. However, standard chemotherapeutic drugs such as vincristine, bleomycin, adriamycin, etoposide, 5-fluorouracil, carboplatin, paclitaxel, and cyclophosphamide can target angiogenesis when the dose and frequency of administration are optimized.[26–29] Continuous low-dose chemotherapy with antitumor drugs was found to be more active against endothelial cells in comparison to tumor cells.[26] Daily administration of topotecan, a camptothecin analog, caused significant tumor growth inhibition associated with a marked decrease in angiogenesis concomitant with HIF-1α inhibition in glioblastoma xenografts.[8] SN-38, an active metabolite of CPT-11, selectively inhibited endothelial cell proliferation and significantly decreased both HIF-1α and VEGF expression of glioma cells in a dose- and time-dependent manner.[30]

In our study, chemosensitive SK-N-AS*nu* and TNB9 were significantly more responsive to daily low-dose CPT-11 treatment than intermittent conventional dosing. Tumor-derived *HIF-1α* and *VEGF* gene expression in TNB9 treated daily with a low dose of CPT-11 were downregulated significantly. However, host-derived *VEGF* gene expression was not suppressed by the treatment. High vascularity was observed in the stromal areas during daily administration of CPT-11. Administration of CPT-11 alone resulted in the incomplete inhibition of tumor growth.

We carried out immunohistochemical experiments for HIF-1α and VEGF in TNB9 and TS-N-2*nu* xenografts. HIF-1α was hardly detected, whereas VEGF was positive in stromal cells in both untreated xenografts. NSE-positive tumor cells were negative for VEGF. In TNB9 treated with CPT-11, both HIF-1α and VEGF were sparsely positive in stromal cells surrounding necrotic areas, whereas VEGF alone was detected in TS-N-2*nu*. In TNB9, VEGF protein expression was induced soon after discontinuation of CPT-11 treatment. VEGF but not HIF-1α expression was closely related to tumor growth inhibition and inhibition of angiogenesis by CPT-11 in NB xenografts. The rapid tumor regrowth of TNB9 xenografts seemed to be the result of an inability to regress host vessels in the stroma during treatment as well as an inability to suppress host-derived VEGF expression. Combined therapy with a persistent blocker of stroma-derived VEGF will be needed to completely block the growth of chemosensitive NB.

Gerber and colleagues reported that complete inhibition of tumor growth and neovascularization in xenografts requires the blockade of both tumor- and host-derived VEGF.[31] They showed that systemic administration of an antihuman VEGF monoclonal antibody with a chimeric murine soluble VEGF receptor protein, mFlt(1–3)-IgG, resulted in complete suppression of tumor growth in a human rhabdomyosarcoma xenograft, indicating that host-derived VEGF significantly contributes to the overall process of tumor angiogenesis and growth.[31]

In TS-N-2*nu*, there was no significant difference in tumor growth inhibition between intermittent conventional-dose CPT-11 treatment and low-dose daily CPT-11 treatment. Both VEGF protein and tumor-derived *VEGF* gene expression levels were not suppressed by low-dose daily CPT-11. Vessels in tumors treated with low-dose CPT-11 were larger and fewer in number than those in untreated tumors; this pattern of results seemed to correspond to the hypoxia-induced apoptosis observed in a large number of TS-N-2*nu* tumor cells. However, NF-positive cells escaped apoptosis and survived. Furthermore, nearly all NF-positive cells were arrested at G_0/G_1 phase. The TS-N-2*nu* tumor cells probably became more aggressive as an adaptation to the hypoxic conditions, resulting in decreased responsiveness to the treatment and increased proliferation. These results show a lack of responsiveness of TS-N-2*nu* xenografts to low doses of CPT-11. Therefore, administration of CPT-11 at a higher dose will be required to inhibit the growth of multidrug-resistant NB.

Acknowledgments

CPT-II was provided by Yakult Honsha. This work was supported by a Grant-in-Aid for Exploratory Research from the Ministry of Education, Culture, Sports, Science and Technology (KAKENHI 19659456). Animal experiments were carried out in a humane manner after receiving approval from the Institutional Animal Experiment Committee of the University of Tsukuba, and in accordance with the university's Regulation for Animal Experiments as well as the Fundamental Guideline for Proper Conduct of Animal Experiment and Related Activities in Academic Research Institutions set forth by the Ministry of Education, Culture, Sports, Science and Technology.

References

1 Komuro H, Li P, Tsuchida Y *et al.* Effects of CPT-11 (a unique DNA topoisomerase I inhibitor) on a highly malignant xeno-transplanted neuroblastoma. *Med Pediatr Oncol* 1994; **23**: 487–92.

2 Shitara T, Shimada A, Tsuchida Y *et al.* Successful clinical response to irinotecan in relapsed neuroblasatoma. *Med Pediatr Oncol* 2003; **40**: 126–8.

3 Tsuchida Y, Shitara T, Kuroiwa M *et al.* Current treatment and future directions in neuroblastoma. *Indian J Pediatr* 2003; **70**: 809–12.

doi: 10.1111/j.1349-7006.2008.00790.x

4 Inagaki J, Yasui M, Sakata N *et al*. Successful treatment of chemoresistant stage 3 neuroblastoma using irinotecan as a single agent. *J Pediatr Hematol Oncol* 2005; **27**: 604–6.
5 Kunimoto T, Nitta K, Tanaka T *et al*. Antitumor activity of 7-ethyl-10-[4-(1-piperidino)-1-piperidino] carbonyloxy-camptothecin, a novel water-soluble derivative of camptothecin, against murine tumors. *Cancer Res* 1987; **47**: 5944–7.
6 Hsiang YH, Hertzberg R, Hecht S *et al*. Camptothecin induces protein-linked DNA breaks via mammalian DNA topoisomerase I. *J Biol Chem* 1985; **260**: 14 873–8.
7 Rapisarda A, Uranchimeg B, Sordet O *et al*. Topoisomerase I-mediated inhibition of hypoxia-inducible factor 1: mechanism and therapeutic implications. *Cancer Res* 2004; **64**: 1475–82.
8 Rapisarda A, Zalek J, Hollingshead M *et al*. Schedule-dependent inhibition of hypoxia-inducible factor-1α protein accumulation, angiogenesis, and tumor growth by topotecan in U251-HRE glioblastoma xenografts. *Cancer Res* 2004; **64**: 6845–8.
9 Wang GL, Jiang BH, Rue EA *et al*. Hypoxia-inducible factor 1 is a basic-helix-loop-helix-PAS heterodimer regulated by cellular O_2 tension. *Proc Natl Acad Sci USA* 1995; **92**: 5510–14.
10 Huang LE, Gu J, Schau M *et al*. Regulation of hypoxia-inducible factor 1 alpha is mediated by an O_2-dependent degradation domain via the ubiquitin–proteasome pathway. *Proc Natl Acad Sci USA* 1998; **95**: 7987–92.
11 Jaakkola P, Mole D, Tian YM *et al*. Targeting of HIF-α to the von Hippel-Lindau ubiquitylation complex by O_2-regulated prolyl hydroxylation. *Science* 2001; **292**: 468–72.
12 Demidenko ZN, Rapisarda A, Garayoa M *et al*. Accumulation of hypoxia-inducible factor-1α is limited by transcription-dependent depletion. *Oncogene* 2005; **24**: 4829–38.
13 Semenza GL. HIF-1: mediator of physiological and pathophysiological responses to hypoxia. *J Appl Physiol* 2000; **88**: 1474–80.
14 Toi M, Matsumoto T, Bando H. Vascular endothelial growth factor: its prognostic, predictive, and therapeutic implications. *Lancet Oncol* 2001; **2**: 667–73.
15 Iyer NV, Kotch LE, Agani F *et al*. Cellular and developmental control of O_2 homeostasis by hypoxia-inducible factor 1 alpha. *Genes Dev* 1998; **12**: 149–62.
16 Ryan HE, Lo J, Johnson RS. HIF-1α is required for solid tumor formation and embryonic vascularization. *EMBO J* 1998; **17**: 3005–15.
17 Carmeliet P, Dor Y, Herbert JM *et al*. Role of HIF-1α in hypoxia-mediated apoptosis, cell proliferation and tumor angiogenesis. *Nature* 1998; **394**: 485–90.
18 Komuro H, Kaneko S, Kaneko M *et al*. Expression of angiogenic factors and tumor progression in human neuroblastoma. *J Cancer Res Clin Oncol* 2001; **127**: 739–43.
19 Meitar D, Crawford SE, Rademaker AW *et al*. Tumor angiogenesis correlates with metastatic disease, N-myc amplification, and poor outcome in human neuroblastoma. *J Clin Oncol* 1996; **14**: 405–14.
20 Ribatti D, Marimpietri D, Pastorino F *et al*. Angiogenesis in neuroblastoma. *Ann NY Acad Sci* 2004; **1028**: 133–42.
21 Geran RI, Greenberg NH, MacDonald MM *et al*. Protocols for screening chemical agents and natural products against tumors and biological systems. *Cancer Chemother Rep* 1972; **3**: 51–61.
22 Ovejera AA, Houchens DP, Barker AD. Chemotherapy of human tumor xenografts in genetically athymic mice. *Ann Clin Lab Sci* 1978; **8**: 50–6.
23 Chomczynski P, Sacchi N. Single-step method of RNA isolation by acid guanidinium thiocyanate–phenol–chloroform extraction. *Anal Biochem* 1987; **162**: 156–9.
24 Pezzolo A, Parodi F, Valeria M *et al*. Tumor origin of endothelial cells in human neuroblastoma. *J Clin Oncol* 2007; **25**: 376–83.
25 Gerdes J, Lemke H, Baisch H *et al*. Cell cycle analysis of a cell proliferation-associated human nuclear antigen defined by the monoclonal antibody Ki-67. *J Immunol* 1984; **133**: 1710–15.
26 Schirner M, Hoffmann J, Menrad A *et al*. Antiangiogenic chemotherapeutic agents: characterization in comparison to their tumor growth inhibition in human renal cell carcinoma models. *Clin Cancer Res* 1998; **4**: 1331–6.
27 Bello L, Carrabba G, Giussani C *et al*. Low-dose chemotherapy combined with an antiangiogenic drug reduces human glioma growth *in vivo*. *Cancer Res* 2001; **61**: 7501–6.
28 Drevs J, Fakler J, Eisele S *et al*. Antiangiogenic potency of various chemotherapeutic drugs for metronomic chemotherapy. *Anticancer Res* 2004; **24**: 1759–63.
29 Kieran MW, Turner CD, Rubin JB *et al*. A feasibility trial of antiangiogenic (metronomic) chemotherapy in pediatric patients with recurrent or progressive cancer. *J Pediatr Hematol Oncol* 2005; **27**: 573–81.
30 Kamiyama H, Takano S, Tsuboi K *et al*. Anti-angiogenic effects of SN38 (active metabolite of irinotecan): inhibition of hypoxia-inducible factor 1 alpha (*HIF-1α*/vascular endothelial growth factor (VEGF) expression of glioma and growth of endothelial cells. *J Cancer Res Clin Oncol* 2005; **131**: 205–13.
31 Gerber HP, Kowalski J, Sherman D *et al*. Complete inhibition of rhabdomyosarcoma xenograft growth and neovascularization requires blockade of both tumor and host vascular endothelial growth factor. *Cancer Res* 2000; **60**: 6253–8.

■ 特集 小児がん治療の晩期障害と対策

進行神経芽腫の両腎温存手術

金子道夫* 平井みさ子 大川治夫 澤口重徳

はじめに

神経芽腫の治療は，限局性腫瘍には手術が，転移性腫瘍には化学療法で原発巣・転移巣，とくに後者をコントロール後に腫瘍全摘とリンパ節郭清が行われ，施設によりその後に放射線治療や幹細胞移植を伴った抗癌剤大量療法が行われている。わが国では限局性腫瘍であっても遺残腫瘍がある場合には化学療法が行われてきたが，最近の欧米での限局性腫瘍に対する治療方針は多少の遺残腫瘍があっても手術のみで90%以上の長期生存が得られており，手術のみで十分であると報告されている。局所進展例で手術困難症例では手術時期を遅らせた delayed surgery が定着した。手術術式は原発腫瘍を全摘し，リンパ節転移に対しては腸骨動脈から横隔膜脚までの系統的リンパ節切除を行う radical surgery が主流である。しかし，筑波大学では1985年の厚生省班研究が開始されて以来，術後直ちに化学療法が開始できるよう系統的リンパ節切除を避け，両腎を温存し，可能な限り術中照射を併用する術式を行ってきた[1]。それまでは骨転移のある症例の予後は絶対不良であったが，その後生存例が得られたことより，長期障害を回避する観点からも有用な方法であると考えている。これらの成績を述べつつ，現時点での神経芽腫治療の問題点，とくに外科治療の問題点とこれからの解決法について述べる。

Ⅰ．進行症例に対する患側腎温存手術 —筑波大学の経験

腹部原発の進行神経芽腫は原発巣とリンパ節が一塊となり腹部大動脈とその主要分岐を取り巻くように進展し，全摘はきわめて困難である。いわゆる「癌の根治手術」は不可能である。化学療法により腫瘍が縮小すると，副腎原発例では原発腫瘍がリンパ節転移とある程度離れ，原発巣は全摘可能となることも少なくない。しかし，後腹膜原発腫瘍は通常転移リンパ節と一塊となり，縮小後も原発腫瘍の同定が困難である。術前化学療法により，易出血性であった腫瘍は硬化して出血は少なくなるが非常に硬くなり，脈管からの剝離は難しく，自律神経やリンパ管とともに血管の外膜層で剝離するのが最も容易で，腫瘍の「全摘」に近い手術が可能である。現在，わが国でも欧米でもこのような手術が行われている。しかし，それでも全摘は困難な症例があり，また，「全摘」してもいわゆる癌の根治的手術とはいえず，またそのような手術では術後の短期的・長期的障害も多くなる。

筑波大学では1985年から厚生省班研究プロトコールに従って化学療法を行い，ほとんどすべての症例で初期治療6クールを終了してから手術を行っている。当時，術前化学療法で切除可能と外科医が判定した時期が手術時期とされ，通常3クール後くらいに摘出術が行われていた。筑波大学では次第に手術時期が遅くなる傾向が顕著であった。手術法は原発巣は全摘，リンパ節は主要な血管を損傷しないようにしてなるべく切除し(図1)，切除後術中照射を併用した。1990年頃からは大きいリンパ節をサンプリングするにとどめた。全例で患側腎の温存をはかり，とくに腎血管や腎門部のリンパ節転移は細心の注意を払って腎の温存に努めた。

* 筑波大学臨床医学系小児外科
〔〒305-8575 つくば市天王台1-1-1〕

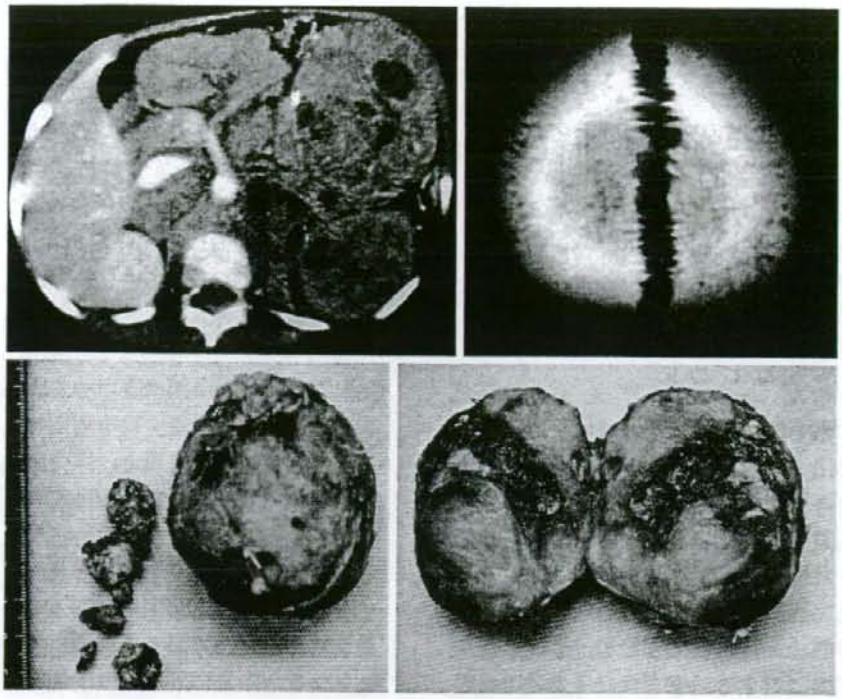

図 1 5歳の腹部原発進行神経芽腫
腹部は多数の腫瘤で占められていた。頭蓋転移も非常に高度であった。初期治療で縮小し，摘出標本はほとんどが神経節腫となった原発巣と 1.5 cm 以上のリンパ節が 3 個，それ以下が 2 個。この患者はその後骨転移再発と照射野外の再発がみられた。

1．手術成績

2005 年までに厚生労働省班研究プロトコールで治療が開始され，3 年以上経過した腹部原発手術症例は 22 例であった。腎は 2 例で腫瘍による水腎症がみられた。また，1 例は患側腎全体に瀰漫性に腫瘍浸潤があり，当初非ホジキンリンパ腫と診断された例では手術時患側腎が全く無機能であったので，当初から腎は合併切除する方針とした。スケジュールの関係で術中照射を施行できなかった 2 例では，リンパ節切除が他の例より広範に施行された。術中照射は 1980 年代では 15 Gy，以後 1995 年までは 12 Gy，それ以後は 10 Gy と減少した。手術もこの 20 年間に変化しており，初期の症例では腎動静脈や腎下部大動脈にかなりの剝離操作を行ったが，1990 年以降は 1.5〜2 cm 以上のリンパ節のみ切除，それがない場合には画像で中心的に存在した部位の組織を生検するのみとした。照射野は術前画像診断により「腫瘍床」に照射し，腎門部にも照射するため一部腎組織に照射される症例もあった。しかし，横隔膜脚より上方は肝臓があるため，技術的制約があり，腫瘍があった部位であっても照射野から外れる症例もあった。術後照射は 1987 年 1 月に手術を行い，病期 4 の最初の生存例となった 1 例で行ったのみである。

2．治療結果

N-myc 遺伝子増幅例の多くは治療に良く反応したが，2 例で初期治療 5 および 6 クールで局所，および転移巣ともに再燃し手術に至らなかった。腹部原発で手術に至った症例は 22 例であった。術中照射を行わなかった 2 例のうち 1 例で，術後 1 年以上にわたり腸管運動異常が持続し，術後化学療法中に腸管からの bacterial translocation と考えられる敗血症をきたした。2 cm 以上の大きなリンパ節が上腸間膜動脈を取り囲んで摘出困難であった 2 例で，骨転移などが遠隔再発し

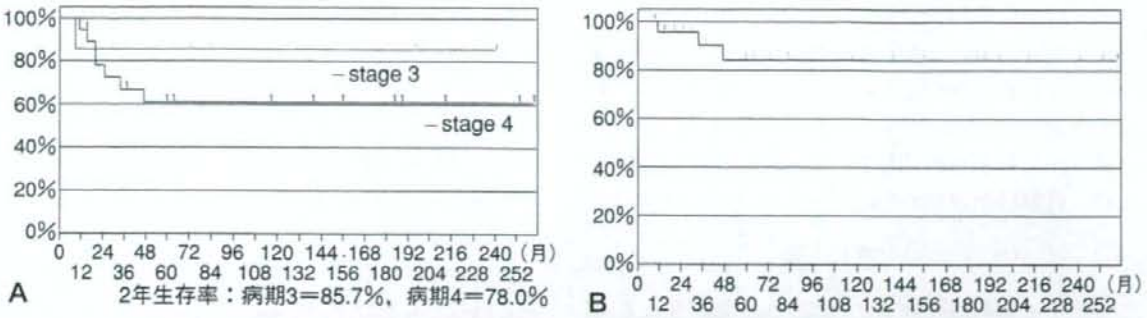

図 2　A. 筑波大学の進行神経芽腫の治療成績（1986～2005 年），**B. 局所コントロール率**
非常に満足すべき結果といえよう。この集計後 1 例が照射野外再発をきたした。

たときに残存リンパ節の増大がみられた。また，照射野外上方から腫瘍が再発し，その後手術野まで進展した症例が 2 例みられた。遺残リンパ節増大 2 例と照射野外からの進展 2 例の計 4 例で「局所再発」が認められた。術後 2 年以上の観察で腫瘍死は 6 例，stage 4 の 5 年生存率 70%，10 年生存率が 61%であった（図 2）。「局所再発」が死亡の原因となった症例はなかった。2 例の腸閉塞を除き合併症，後障害を認めていない。

3．腎温存の結果

腫瘍の広範な腎進展で術前無機能となった 1 例を除き，全例で両側腎温存手術が行われた。水腎症 2 例のうち 1 例において術後 4 年で腎盂尿管移行部狭窄による水腎症の悪化がみられ，腎杯尿管吻合術を施行した。主に CDDP によると考えられる治療中のクレアチニンクリアランスの低下が多くの症例でみられ，造血幹細胞移植などでの抗癌剤投与量を調節した症例が認められたが，腎機能障害による治療の中止症例はみられなかった。ただし，生存例のほとんどでβ_2ミクログロブリンの異常が現在も認められるが，これは手術の影響ではなく，抗癌化学療法のためと考えられる。術中照射による椎体，脊髄の障害は術後照射を併用した 1 例を除いてみられなかった。分腎機能についての検討は一部の症例以外に行われておらず，今後の重要課題と考えられる。

病期 4 での筑波大学生存第 1 例は腎機能の観点から示唆に富むので報告したい。

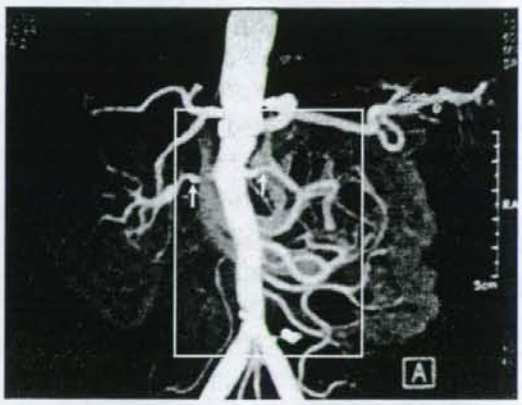

図 3　長期生存第 1 例目の治療後 19 年後
四角い枠は照射野で，腹部大動脈に発育不全がみられ，右腎動脈は高度の狭窄になっている。左腎動脈は全長にわたって細い。左腎は水腎症で，実質が薄くなっている。

症　例

4 歳 1 カ月，女児

左後腹膜原発病期 4 で，腫瘍による左水腎症が明らかであった。85A1 6 クール終了後，治療開始後 6 カ月で，腫瘍切除が行われた。腫瘍は 45×35×23 cm で，腫瘍床に対し術中照射 12 cm×6 cm の照射野に 15 Gy 施行した。術後 6 日目より，腫瘍床，傍大動脈，腎門部の椎骨レベルで Th_{11}～L_4に対し，6MeV の X 線 1 回 1.8 Gy，総線量 14.4 Gy の外部照射を施行した。術後化学療法（85A2 および 85C）を 5 クール施行後，帯状疱疹となったため治療終了とした。その後再発は認められなかったが，手術後 7 年経過して左水腎症の進行が

みられ，腎盂尿管移行部狭窄切除・腎杯尿管吻合術を施行した。治療開始後 19 年経過後，高度の高血圧に偶然気づき，精査したところ照射した大動脈およびその主要分岐に発育不全による高度の狭窄が発見された（図 3）。腎血管の再建は困難で腎の自家移植が勧められているが，未施行である。

II．考　察

厚生労働省班研究プロトコールが施行される前までは，有効な治療レジメンがないこともあり，大きな局所腫瘍に対しチャレンジングな癌の手術が行われ，患側腎の合併切除もやむを得ないものと考えられた。しかし，85 プロトコールにより原発腫瘍がかなり縮小することが多くなり，1990 年代に入り患側腎温存は次第に受け入れられるようになった。今では腎温存が標準的術式になったと思われる。しかし，温存したはずの腎が術後に消失したり，大幅な機能喪失をきたすことが少なからずあり，これは腎血管に対するリンパ節郭清により腎血管の損傷や攣縮のために術後血行障害に陥るためである。時に両側腎が血行障害になる。上腸間膜動脈や腹腔動脈でも同様であり，さらに血管に密にからみつくように存在する自律神経やリンパ管が切除されることにより，術後の腸管運動不全や大量のリンパ漏のため，術後化学療法の施行にも大きな影響がある。さらに，これまで治癒不能な進行神経芽腫にも生存例が得られるようになり，系統的リンパ節郭清は今後男子の性機能不全など新たな長期障害となる可能性が高い。

欧米でも進行例に系統的リンパ節郭清を行う意義を疑問視する外科医は少なからず存在するが，腫瘍全摘症例と遺残症例で治療成績が前者で有意によいとの観察から，進行例であっても腫瘍全摘を目指し，リンパ節郭清を行う術式が多数派である。しかし，術式の層別化を行った臨床試験は実際は困難で，科学的エビデンスを証明することはいまだなされていない。これまで，適切な局所治療の臨床試験は困難とされていたが，2006 年から開始された進行神経芽腫に対する臨床試験では局所治療を治療の最後におき，手術の方式も系統的リンパ切除を行わない術式に統一した。これにより，局所治療の意義とこの術式を明らかにし，さらに，治療の最後に摘出した腫瘍の病理組織と再発との関連をみることができるプロトコールとなっている。以下にそのプロトコールの腹部での外科治療の部分を概説する。

1．外科治療

high-risk 群に分類される 1 歳以上の病期 3，4 の神経芽腫は，化学療法で縮小が得られても完全摘除が非常に難しく，厳密には完全摘除は不可能といっても誤りではない。しかし，多くの施設でより高い根治性を目指して可能な限り切除を行うことに努力してきた[2~5]。神経芽腫の進展様式からいって，完全切除を目指す手術は血管およびその周囲の神経組織，リンパ管の損傷を伴い，術後腹部腫瘍臓器の血行障害，腸管の運動障害，術後の大量リンパ瘻，呼吸不全の問題も常に伴っていた[6,7]。とくに，腎の血行障害は化学療法剤の変更，減量さらに引き続いて施行される大量化学療法のリスクを大きく左右する。手術のこれらの問題は術後化学療法の開始時期の遅れ，投与抗癌剤の減量，腎障害など，術後治療のばらつきの大きな要因になり，適切な治療法を明らかにする臨床試験の遂行を妨げる大きな要因となった。いくつかの施設では術中照射法や術後照射と組み合わせることにより，より侵襲の少ない手術とする治療方針をとり，それにより局所再発率を高めることはないとの報告がみられる[8~10]。

2．原発巣摘除と機能温存

進行神経芽腫は治療成績がまだ不良とはいえ，5 年生存率は 40%に達する。したがって，局所再発の頻度を上げることなく機能温存を考慮することは重要である。また，治療中の合併症を少なくし，治療を予定どおり完遂するためにも短期合併症を防止することは治療成績向上に資すると考えられる。以下に進行神経芽腫の外科治療ガイドラインのうち腹部に関する部分を掲げる。

1）原発巣に関して

原発部位にかかわらず，原則として周囲臓器をできるだけ温存して原発巣を全摘出する。原発巣と一塊になったリンパ節は原発巣とともに切除を目指す。

(1) 副腎，後腹膜原発：肝・腎に関しては，手術時に viable とみられる浸潤がある場合は，部分

合併切除を行う。

(2) 機能のある腎は温存する。腎血管を巻き込んでいて剝離が困難な場合，腫瘍被膜内切除にて腎血管を温存し，腎合併切除を極力避ける。腎動脈の攣縮にはキシロカインを浸したガーゼで包み，攣縮を軽減しつつ手術を続行し，腎温存につとめる。

(3) 広範な腎実質浸潤がある場合には，腎合併切除をする。腎合併切除を行っても，腫瘍全摘出困難な場合は，腎を温存して，できるだけ腫瘍切除を行う。

(4) 腹腔動脈や上腸間膜動脈などの腹部大動脈からの主要な血管を巻き込んでいて剝離が困難な場合は，腫瘍被膜内切除にて血管を温存してできるだけ腫瘍を切除するものとする。

2) 転移巣に関して

(1) 原則として系統的リンパ節郭清は行わないものとする。

(2) 転移リンパ節と思われる 2.0 cm 以上のリンパ節は切除する。それ以下の大きさであっても肉眼・触診上で viable とみられる腫瘍があると考えられるリンパ節は切除する。

(3) 2.0 cm 以上のリンパ節の腫大したリンパ節が手術時にない場合，治療前に転移のみられた部位のリンパ節サンプリングを行う。

おわりに

筑波大学で 20 年間にわたり施行された，腹部原発進行神経芽腫の手術について報告した。これらはほぼ一貫して両側腎の温存につとめ，局所制御でも生存率でも満足できる結果が得られた。現在行われている臨床試験では手術に関しこのコンセプトで施行されている。ただし，術中照射が可能な施設は限られているので，術中照射に代わり術後外部照射が施行される。その結果が，筑波大学とほぼ同じ結果が得られれば，世界に発信できる成果になる。術中照射の照射量に関しては線量が次第に少なくなってきており，血管系の長期障害が千葉大学から報告されている。成長する小児にあっては予想外の長期障害が出現する可能性があり，現在筑波大学症例でも長期障害調査が進行中である。

文 献

1) Kaneko M, Ohkawa H, Iwakawa M : Is extensive surgery required for the treatment of advanced neuroblastoma? J Pediatr Surg **32** (11) : 1616-1619, 1997
2) Tokiwa K, Fumino S, Ono S, et al : Results of retroperitoneal lymphadenectomy in the treatment of abdominal neuroblastoma. Arch Surg **138** (7) : 711-715, 2003
3) Kuroda T, Saeki M, Honna T, et al : Clinical significance of intensive surgery with intraoperative radiation for advanced neuroblastoma : Does it really make sense? J Pediatr Surg **38** : 1735-1738, 2003
4) Adkins ES, Sawin R, Gerbing RB, et al : Efficacy of complete resection for high-risk neuroblastoma : a Children's Cancer Group Study. J Pediatr Surg **39** : 931-936, 2004
5) La Qualia MP, Kushner BH, Su W, et al : The impact of gross totaal resection on local control and survival in high-risk neuroblastoma. J Pediatr Surg **39** : 412-417, 2004
6) Rees H, Markley MA, Kiely EM, et al : Diarrhea after resection of advanced neuroblastoma : A common management problem. Surgery **123** : 568-572, 1998
7) Shamberger RC, Smith EI, Joshi VV, et al : The risk of nephrectomy during local control in abdominal neuroblastoma. J Pediatr Surg **33** : 161-164, 1998
8) Kaneko M, Ohkawa H, Iwakawa M : Is extensive surgery required for the treatment of advanced neuroblastoma? Journal of Pediatric Surgery **32** : 1616-1619, 1997
9) Von Schweinitz D, Hero B, Berthold F : The impact of surgical radicality on outcome in childhood neuroblastoma. Eur J Pediatr Surg **12** : 402-409, 2002
10) Castel V, Tovar E, Costa J, et al : The role of surgery in stage IV neuroblastoma. J Pediatr Surg **37** : 1574-1578, 2002

Journal of Pediatric Surgery (2008) 43, 1376–1379

ELSEVIER

Journal of Pediatric Surgery

www.elsevier.com/locate/jpedsurg

A rare case of presacral cystic neuroblastoma in an infant

Miho Watanabe[a,*], Hiroaki Komuro[a], Michio Kaneko[a], Tetsuo Hori[a], Yukihiro Tatekawa[a], Sumi Kudo[a], Yasuhisa Urita[a], Seiichiro Inoue[a], Manabu Minami[b], Masato Sugano[c]

[a]*Department of Pediatric Surgery, University of Tsukuba, Tsukuba, Ibaraki 305-8575, Japan*
[b]*Department of Radiology, University of Tsukuba, Tsukuba, Ibaraki 305-8575, Japan*
[c]*Department of Pathology, University of Tsukuba, Tsukuba, Ibaraki 305-8575, Japan*

Received 14 December 2007; revised 5 February 2008; accepted 13 February 2008

Key words:
Cystic neuroblastoma;
Presacral;
Infant

Abstract Cystic neuroblastoma (CN) is an extremely rare entity, although neuroblastoma is the most common solid tumor in infants. The radiologic diagnosis of CN is very difficult because of both the rarity and minimum solid component of the lesion. We describe herein the case of a 2-month-old girl presenting with dysuria because of a large presacral mass. Imaging studies including ultrasonography, computed tomography, and magnetic resonance imaging demonstrated a large septated cystic tumor mimicking a cystic sacrococcygeal teratoma, which commonly occurs in the presacral region. The tumor was finally diagnosed as CN after surgical resection. This is the second case report of presacral CN in the English literature. Cystic neuroblastoma should be considered in the differential diagnosis of presacral cystic tumors in infants.

Neuroblastoma is one of the most common childhood malignancies. Neuroblastoma usually presents with solid masses and rarely forms cystic masses. The entity of cystic neuroblastoma (CN) is almost exclusively located to the adrenal gland and is rarely seen in other regions. We report an extremely unusual case of presacral CN presenting as urinary retention in a 2-month-old girl.

1. Case report

A 2-month-old girl was referred to our hospital with dysuria and abdominal distension. Physical examination revealed marked distension of the lower abdomen because of the urinary bladder filled with urine. Digital rectal examination disclosed a firm presacral mass behind, causing rectal stenosis. Plain film demonstrated a hemispherical opaque mass in the pelvic space with upward displacement of the intestines (Fig. 1). Ultrasonography demonstrated massive urinary retention and a large presacral cystic mass. Computed tomography (CT) showed a large, presacral cystic mass with septation and megacystis because of the compressed urethra. This cystic tumor was 58 × 42 × 192 mm, comprising 2 cystic lesions divided by fibrous septa and

* Corresponding author. The Children's Hospital of Philadelphia, The Center For Fetal Research, Abramson Pediatric Research Center, 1114H, 3615 Civic Center Boulevard, Philadelphia, PA 19104-4318, USA. Tel.: +1 215 590 1138; fax: +1 215 590 3324.
E-mail address: mihomibow@hotmail.co.jp (M. Watanabe).

0022-3468/$ – see front matter © 2008 Published by Elsevier Inc.
doi:10.1016/j.jpedsurg.2008.02.063

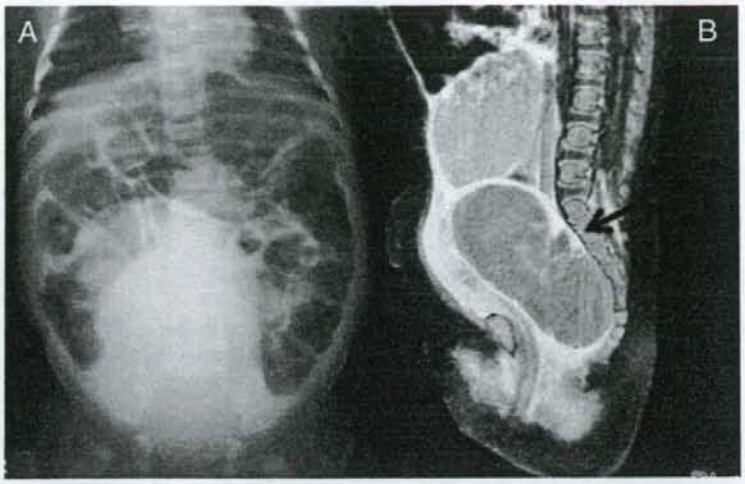

Fig. 1 A, Abdominal radiography on admission. An opaque, hemispherical mass, which contains tumor as well as distended bladder, is apparent in the pelvic space with upward displacement of the intestines. B, Abdominal T1-weighted MRI after urinary catheterization. Tumor consisted of 2 cystic lesions. Fluid-fluid levels with different contrasts are clearly seen in this bilocular cystic mass. Fluid in the upper cystic lesion shows relatively high-signal intensity. Reticular structures suggesting the presence of fibrin (arrow) are observed in the lower cystic part.

surrounded by a thin wall without any obvious solid component or calcification. The dorsal wall of the cyst was slightly enhanced by CT scan, but no tumor vessels were demonstrated. Contents of the bilocular cystic tumor showed fluid-fluid levels.

Findings of the CT scan were suggestive of cystic teratoma or cystic lymphangioma, but inconclusive, so a magnetic resonance imaging (MRI) was obtained. The cyst fluid was intermediate-to-high intensity by a T1-weighted MRI, and the reticular structure protruding from the posterior wall of the cysts was read as blood (Fig. 1B).

The tumor was preoperatively considered as a cystic sacrococcygeal teratoma, which is commonly seen in this region, although no obvious adipose tissue or calcification was detected. Laboratory findings were unremarkable. Levels of tumor markers such as neuron-specific enolase (NSE) and α-fetoprotein were within normal ranges. Urinary levels of vanillylmandelic acid (VMA) and homovanillic acid (HVA) were not analyzed.

The patient was brought to the operating room, and the tumor was excised through an abdominosacral approach. Briefly, the patient is positioned prone, and a 5-cm midline incision was made over the sacrum and coccyx. When the coccyx was separated from the surrounding tissue and sacrum, the lower part of cystic tumor was easily visualized and carefully separated laterally from the pelvic floor and anteriorly from the rectum.

Half of the tumor could be dissected freely. However, the tumor was large and adhered to the sacrum, so that it was impossible to resect it further from the posterior approach. Then with the patient supine, a transverse abdominal incision was made. The bladder and uterus were freed anteriorly from the tumor, and the tumor was fully removed from the sacrum without any injury to surrounding organs (Fig. 2). There was one vessel entering the posterior wall of the tumor, which was ligated. The excised tumor comprised 2 cysts, containing sanguinous and fibrinous exudates.

Pathologic result showed nests of neuroblastic cells in the solid part of the cyst wall (Fig. 3A). Small, round tumor cells with scant cytoplasm showed diffuse and dense infiltrative growth within the fibrous walls. A delicate neurofibrillary matrix center was seen with rosette formation. Calcification was not observed. Tumor cells were positive for CD56/neural cell adhesion molecule (NCAM), synaptophysin,

Fig. 2 Intraoperative view of tumor through the abdominal incision. After dissecting retroperitoneal membrane, dark colored cystic tumor was seen. Bladder and uterine tube were also detected in front of tumor and anteriorly displaced by large tumor.